Materials and Design 186 (2020) 108369

Contents lists available at ScienceDirect

Materials and Design

journal homepage: www.elsevier.com/locate/matdes

Low-velocity impact response of friction riveted joints for aircraft application

N.Z. Borba [a,b], J. Körbelin [b], B. Fiedler [b], J.F. dos Santos [a], S.T. Amancio-Filho [c,*]

[a] Helmholtz-Zentrum Geesthacht, Centre for Materials and Coastal Research, Institute of Materials Research, Materials Mechanics, Solid State Joining Processes, 21502 Geesthacht, Germany
[b] Hamburg University of Technology, Institute of Polymer and Composites, 21073 Hamburg, Germany
[c] Graz University of Technology, Institute of Materials Science, Joining and Forming, BMVIT Endowed Professorship for Aviation, 8010 Graz, Austria

HIGHLIGHTS

- Rivet markedly improved the energy required to extend the impact damage in friction riveted joint.
- Peel stresses mostly induced premature failure of the metal-composite interface and delamination of the composite.
- Prematurely failed interfaces decreased the quasi-static strength and fatigue life of impacted joints.
- Impacted friction riveted joint after high fatigue cycles was more sensitive to impact than to fatigue damage.

GRAPHICAL ABSTRACT

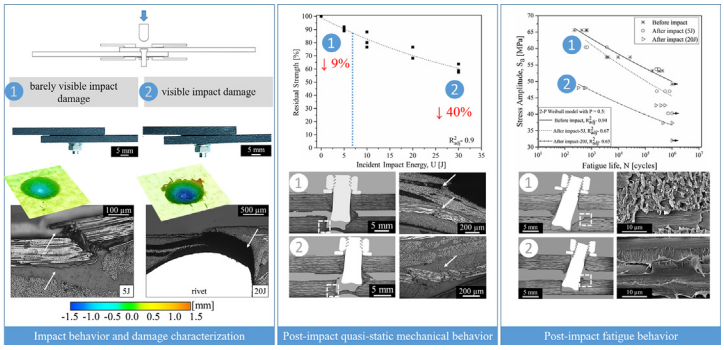

ARTICLE INFO

Article history:
Received 26 September 2019
Received in revised form 31 October 2019
Accepted 14 November 2019
Available online 16 November 2019

Keywords:
Friction riveted joint
Impact damage
Residual strength
Post-impact fatigue life

ABSTRACT

In this paper, the sensitivity of carbon fiber reinforced polyether-ether-ketone (CF-PEEK) friction riveted joints to impact damage was assessed as well as the damage propagation during fatigue and quasi-static mechanical testing. The joints were impacted with energies between 5 J and 30 J at room temperature and the impact damage was evaluated through microscopy and ultrasonic C-scan. Two damage types were identified: barely-visible impact damage with mainly shear-driven damage in the first plies of the composite and visible impact damage with delamination and premature failure of the rivet-composite interface owing to peel stresses upon the impact event. The joint strength and fatigue life were not compromised by the barely-visible impact damage, while a 40% decrease of quasi-static strength and lower fatigue resistance were achieved for visible impact damage. Despite altered fatigue behavior of impacted joints, damage accumulated towards fatigue was not critical to the joint mechanical integrity, confirmed by the residual strength of up to 96% after 10^6 cycles for 20 J impacts.

1. Introduction

Aircraft composite structures, especially the composite fuselage, are prone to impact damage [1]. Contrary to metal structures, carbon fiber reinforced polymers (CFRP) absorbs impact energy mainly through

* Corresponding author.
E-mail address: sergio.amancio@tugraz.at (S.T. Amancio-Filho).

https://doi.org/10.1016/j.matdes.2019.108369

material damage and elastic deformation, instead of plastic deformation [2,3]. The nature of impact damage for aircraft structures is various and has been classified according to the impact velocity [4,5]:

- tool drop during maintenance operations is classified as low velocity – e.g. 4 to 10 m/s – impact event with an impact energy of up to 35 J;
- runway debris impact has an intermediate velocity and impact energies in the order of 50 J;
- bird strike and accidental damage such as the impact of integrated parts are classified as having intermediate velocities of 100 to 150 m/s with impact energies of over 100 J.

In accordance with this classification, Airbus has recently reported an impact damage screening on the A320 fuselage aiming to evaluate the impact threat for the A350XWB composite fuselage [6]. The low-velocity impact events had a higher probability of occurrence throughout the structure and mainly localized around the passenger and cargo doors.

To assess the low-velocity impact damage, drop weight impact testing has been widely used to study the impact behavior of composite structures [2,7–11], adhesive bonded composites [12–14], and metal-composite laminates [15,16]. However, only few investigations have been performed on impacted bolted composite structures, where the considerable increase of stress concentration in the impacted bolted area plays an important role on the joint integrity [17]. Ochôa et al. [17] reported the detection of internal delamination in impacted stringers bolted to CF-PEKK panels of a horizontal stabilizer torsion box by an ultrasonic guided wave monitoring system. However, no investigation of impact damage evolution and residual strength was addressed. Vieille et al. [7] compared the impact damage resistance and tolerance of CF-PEEK, carbon fiber reinforced polyphenylene sulfide (CF-PPS), and carbon fiber reinforced epoxy-based polymers (CF-epoxy) by the size of the impact damage and post-impact compression behavior. The authors reported better impact damage tolerance of a CF-PEEK, which was reflected in a restricted propagation of the impact damage and a 30% higher residual compressive strength than CF-epoxy and 12% higher than CF-PPS. Tai et al. [18] reported a decrease in the fatigue life of CF-PEEK impacted by an energy of up to 25 J and cyclic loading under a tension-tension regime owing to impact-induced delamination. From an ultrasonic C-scan inspection, the authors concluded that the delamination induced by the impact did not grow during fatigue life, leading to no apparent stiffness degradation over the fatigue cycles. With the presence of a metal interlayer in CFRP, additional mechanisms to release the impact energy have been reported [15,16]. Aside from delamination of fiber-matrix interface, adhesive failure of the metal-composite interface along with plastic deformation of the metal layer seems to increase the absorption of impact energy considerably in comparison to CFRP, and so represents a promising strategy for improving the impact resistance of composites [15,16].

Friction riveting has been shown as an alternative joining technology suitable for aircraft composite laminate structures [19–22]. The main advantages of the process in comparison to conventional mechanical fastening variants are its simple machinery, short joining cycles, cleanness, single-process step, and fully automatization which enable cost saving and its transferability to a production line, along with suitability to wide range of lightweight metallic alloys and polymer composites [19,22–25]. Borba et al. [19] recently investigated the mechanical behavior of optimized Ti6Al4V/CF-PEEK friction riveted joint under quasi-static and cyclic loading in comparison to reference bolted joints [26]. Although decrease of 29% of the quasi-static strength, friction riveting showed improvement of 88% of the fatigue life compared to the reference joint, owing to the absence of clearance at the rivet-composite interface, good surface finishing of the composite hole and therefore low notch effect [26]. Despite the deep phenomenological understanding of the process [27,28] along with process-induced microstructural and physicochemical changes of the joint materials, the scale-up of the process to aircraft composite structures is still impaired by knowledge gaps in accidental damage threat and its effect on the joint mechanical integrity. Therefore, this work evaluates for the first time the impact damage resistance and tolerance of friction riveted joints. A case study overlap joint using aircraft-relevant materials (Ti6Al4V rivets and CF-PEEK parts) was investigated. The joints were subjected to different impact energies within a range of low-velocity impacts and the damage size was investigated for the minimum and maximum impact levels through non-destructive ultrasonic method and microscopy. In addition, the post-impact mechanical performance of the joints under quasi-static and cyclic loadings was addressed, including the damage propagation description through stiffness degradation analysis.

2. Materials and methods

2.1. Materials and joining procedure

Single overlap joints were produced using a FricRiveting gantry system (RNA, H. Loitz-Robotik, Germany) coupled with a pneumatic clamping system, where the composite parts were fixed. The samples comprised two 4.34 mm (nominal thickness) overlapped CF-PEEK laminates with 58 wt% nominal fiber content in a stacking sequence of $[[(0,90)/(\pm 45)]_3/(0,90)]_s$ (Toho Tenax Europe GmbH, Germany) and joined with extruded plane rivets of Ti6Al4V (Henschel KG, Germany) with a diameter of 5 mm and a length of 60 mm, as schematically shown in Fig. 1. The M5 stainless steel nut and washer were externally tightened with 1.0-Nm torque to pre-load the joints—this is carried

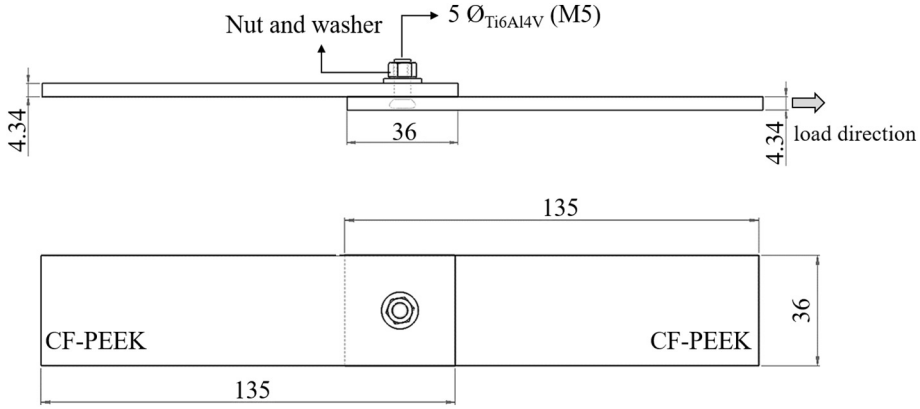

Fig. 1. Schematic illustrations of a single lap shear specimen geometry along with the dimensions and load direction (all dimensions are in millimeters).

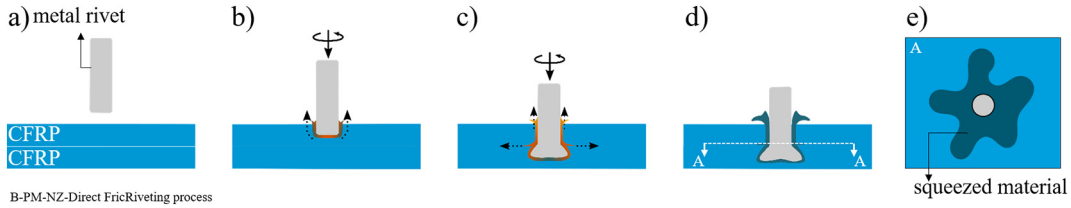

Fig. 2. Direct friction riveting steps at different joining stages. a) positioning of the joining parts; b) rivet rotation and insertion through the upper composite (CFRP) part; c) rivet insertion through the lower CFRP part and rivet tip plastic deformation; d) joint consolidation (adapted from [19]); e) schematic illustration of the squeezed material.

out to minimize through-thickness failure and consequently maximize the joint load capacity [29].

Direct friction riveting, a process variant of friction riveting, was used to join the CF-PEEK parts and the Ti6Al4V rivet. The friction riveting process is thoroughly described in previous publications [23,30,31], while the direct friction riveting process was recently published in [19,20] and applied for an overlap joint configuration. Fig. 2 schematically depicts the joining stages. In brief, direct friction riveting consists of frictional heat generated through the rotating rivet insertion into overlapping composite plates, leading to the plasticization of the rivet tip and its plastic deformation under an increased axial force and its consequent anchoring within the composite plates. Moreover, the high shear rate and process temperature – between 60% and 90% of the metallic meting point – leads to metallurgical transformations while the composite part undergoes partial thermo-mechanical decomposition, fiber breakage, reduction of matrix viscosity, and crystallinity decrease, as reported by Borba et al. [19] for Ti6Al4V/CF-PEEK friction riveted joints. During the joining, part of the molten polymer matrix is squeezed between the composite parts and flows towards the overlap's upper surface which promote adhesion forces and joint sealing at the metal-composite and composite-composite interfaces after polymer consolidation. The adhesion together with the rivet anchoring into the composite parts are the main bonding mechanisms of overlap friction riveted joints. Fig. 3 exemplified a typical cross-section of Ti6Al4V/CF-PEEK friction riveted joint, showing the absence of delamination in the joining area (Fig. 3-b) as well as the embedding and reconsolidation of fibers and matrix at the metallic surface (Fig. 3-c). Due to the controlled heat generation, thermal effect in the metal-composite interface is less extensive [19]. Nonetheless a few volumetric defects, such pores, are encountered in the metal-composite interface in comparison to conventional polymer welding processes; in friction riveting the majority of degraded composite matrix is expelled in form of flash material, reducing the presence of volumetric defects in the consolidated area.

The direct friction riveting process was optimized for the selected base materials by 2^3 full-factorial design of experiments and analysis of variance. The results of the process optimization and the influence of all process parameters on the mechanical strength of friction riveted joints is beyond the scope of this work and will be published elsewhere. Nonetheless, the joining parameters range used to perform the experiments were: rivet rotational speed from 10,000 rpm to 15,000 rpm, friction force from 10 to 15 kN, and clamping pressure from 0.2 to 0.6 MPa. A desirability function was used to select the adequate set of joining parameters that comply with the target of maximized ultimate lap shear force. The following set of parameters where used: rivet rotational speed of 15,000 rpm, friction force of 5 kN and 10 kN during the rivet insertion through the upper and lower composite parts respectively, displacement at friction of 7.5 mm, consolidation time of 10 s, and clamping pressure of 0.2 MPa.

2.2. Global mechanical properties

2.2.1. Drop weight impact testing

To study impact damage tolerance of the friction riveted joints, drop weight impact tests were carried out using an instrumented drop tower, following the ASTM D7136 [32] standard, at room temperature. Fig. 4 illustrates the set-up for the drop weight impact test. The specimen geometry is depicted in Fig. 1. A pneumatic clamping system made out of steel with a 15 mm diameter circular window was employed to ensure reproducibility of the testing conditions. This clamping consists of a circular plate with fixed edges. A hardened steel dart impactor with a hemispherical 12.5 mm diameter tip fixed to the weight was used to impact the center of the joint's back surface. An anti-rebound system was coupled to the drop tower, to prevent multiple impacts during testing. The incident impact energies (U) of 5 J, 10 J, 20 J, and 30 J were selected within a range of low-velocity impact events with high probability of occurrence on the A320 fuselage, as reported by Airbus [6]. Four replicates were tested for each level. The impact energies were achieved by varying the drop weight, while the height was kept constant at 300 mm. The load over time was acquired and used to calculate the absorbed energy (U_t).

2.2.2. Quasi-static mechanical testing

Single lap shear (LS) testing was carried out to assess the residual quasi-static mechanical performance of joints post impact. The joint strength was evaluated in accordance with ASTM D5961 [33] using a universal testing machine (model 1478, Zwick Roell, Germany) with a load capacity of 100 kN. The test speed was 2 mm/min and testing was performed at room temperature (21 °C). The average ultimate lap shear force (ULSF) of non-impacted and impacted joints was obtained from three test replicates for each impact energy level.

2.2.3. Fatigue testing

The post-impact fatigue life of the joints was accessed through fatigue testing which was carried out using a servo-hydraulic machine (Instron/Schenck, Germany) with ±10 kN load capacity in a tension-tension regime at stress ratio of $R = 0.1$. A constant amplitude

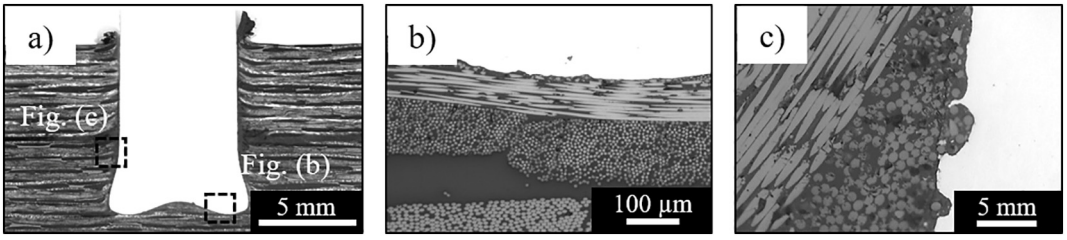

Fig. 3. a) Typical friction riveted joint cross-section of Ti6Al4V rivet and CF-PEEK overlapped plates. Interfaces between the metallic rivet and the composite in the joint area showing b) absence of composite delamination and c) fiber and matrix embedment in the metallic surface.

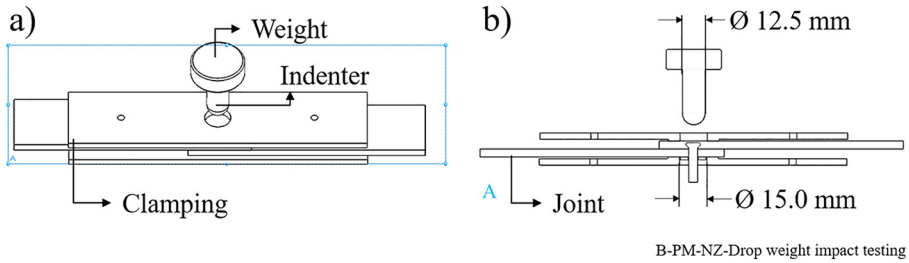

Fig. 4. a) Set-up of the drop weight impact test; b) neutral plane of the set-up, showing the dimensions of the indenter and the inner diameter of the ring from the clamping system.

sinusoidal loading at a frequency of 5 Hz was set. Load levels of 60%, 70%, 80%, and 90% of the joint's residual strength were used to determine the Wöhler (S-N) curve. According to the guideline provided by ASTM E739 [34], a minimum number of specimen of 6 to 12 and replication percentage (% replication = 100 [1 − (total number of different stress or strain levels used in testing/total number of specimens tested)]) of 33 to 50% are considered adequate for research and development purposes, which guarantee a reliable characterization of fatigue behavior. In this work, four replicates for each stress level – i.e. 16 specimens – were tested to analyze the fatigue behavior before impact while three replicates for each stress level – i.e. 12 specimens – were tested to analyze the fatigue behavior after impact, which corresponded to 75% and 67% of replication, respectively. A Weibull distribution was used to model fatigue life of the friction riveted joints according to the DIN 50100:2016-12 [35] standard. Complete joint failure and the joint withstanding 10^6 cycles were used as indications to cease the tests. The joints that survived 10^6 cycles without failure (termed run-out specimens) were subsequently tested under quasi-static conditions, as described in Section 2.2.2, and their residual strength reported. A variation in the joint stiffness was used as an indication of damage accumulation throughout the joint fatigue life. The stiffness degradation was calculated as $D = 1 - (E/E_0)$, with E_0 the initial joint stiffness.

2.3. Damage characterization

The non-impacted and impacted joints were primarily inspected by ultrasonic (US) C-scan (USPC 3040 DAC, Dr. Hilger Ingenieurbüro, Germany) which has 20 MHz resolution, and coupled with a 6 MHz ultrasonic testing probe (Karl Deutsch GmbH, Germany). The pulse-echo method was adopted, which is characterized by a single transducer working as both transmitter and signal detector. The coupling medium was demineralized water while the ultrasound speed was calibrated based on the sample thickness. The signal detected during measurement was plotted as a function of position, providing what is known as an amplitude C-scan display. Fig. 5-a and -b show the set-up for the US measurement. The bottom surface of the lower composite plate was scanned, while the upper composite plate was defined as a backing — i.e. ultrasound signals from this region were rejected. Fig. 5-c shows a typical defect's depth measurement of an as-joined friction riveted joint, where the position of the rivet tip into the lower composite plate is highlighted by a circle of dashed lines. All the samples were dried after US C-scan for further analyses.

Confocal laser scanning microscopy (CLSM) was used to access three-dimensionally the permanent deformation introduced by the drop weight impact testing. The impact area (A_i) and the residual dent depth (d) were measured. Additionally, light optical microscopy (LOM; DM IR microscope, Leica, Germany) was employed to analyze the microstructure of the joints' cross-section, while scanning electron microscopy (SEM; Quanta™ FEG 650 equipment, FEI, USA) was employed for fractography. The joint cross-sections were prepared following a standard materialographic procedure: joints were sectioned through the center of the rivet, embedded in cold resin, ground and polished to obtain a smooth surface finishing. For SEM analysis, the conductivity of the sample surfaces was improved via gold sputtering using a Q150R ES equipment (Quorum Technologies Ltd., UK) for 15 s with a current of 65 mA. The imaging of the fracture surface was performed with voltage of 10 kV, the spot size of 3.5, and working distance of 25 mm.

3. Results and discussion

3.1. Impact loading and energy history

Fig. 6 shows typical curves of contact force (impact force) and energy history as a function of time for four levels of impact energy. The incipient damage point (IDP), maximum load point (MLP), failure point (FP), and total point (TP) were detected and used to assess the impact response and resistance of the composite friction riveted specimens. The IDP is characterized by the incipient damage load (P_i) and energy (U_i) which indicate the ability of a structure to withstand the damage and deformation initiation [36]. The MLP contains the peak force (P_m) that a composite structure can tolerate before undergoing critical damage which leads to reduction of sample rigidity and failure during a particular impact event [37,38]. The energy at the maximum

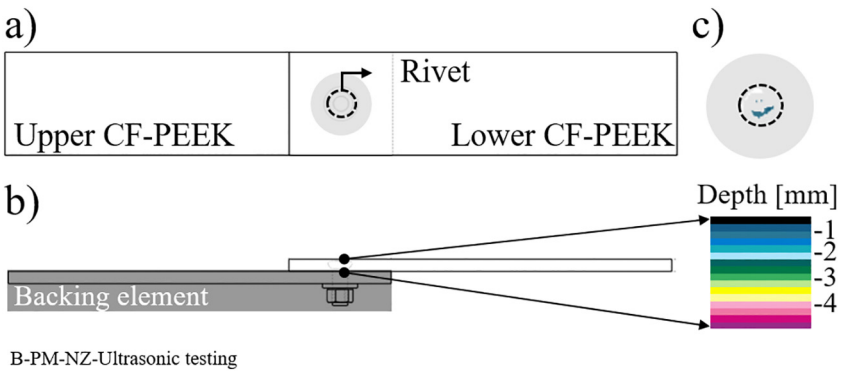

Fig. 5. a) Schematic illustration of the bottom view of the joint, highlighting the region of US measurement; b) side view of the friction riveted joint, showing the selected backing surface and the scale of the defect depth based on the lower composite thickness; c) typical cross-sectional view of the as-joined friction riveted joint along with US measurement.

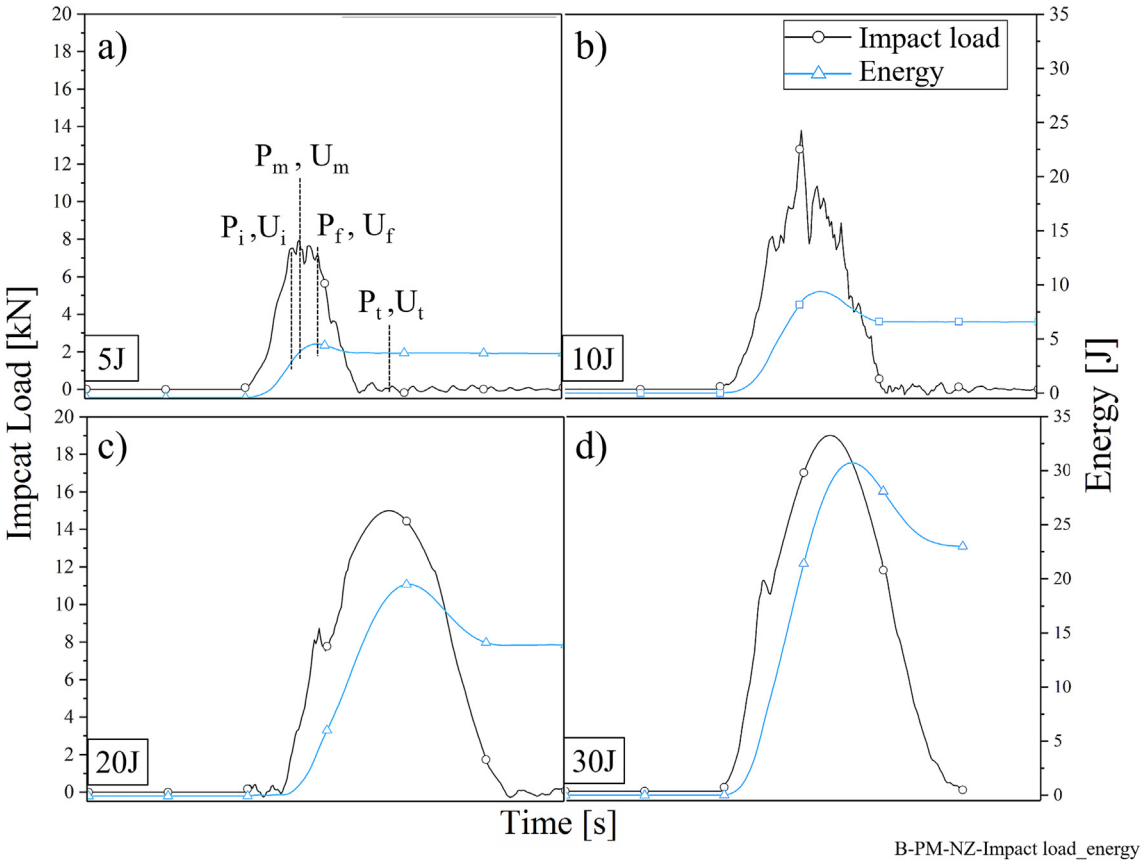

Fig. 6. Typical impact load and energy curves as a function of time for incident impact energies of a) 5 J, b) 10 J, c) 20 J, and d) 30 J.

load (U_m) therefore can be interpreted as the required energy to induce elastic-plastic deformations through flexural deformation and interlaminar shear [36]. At the FP, characterized by maximum energy (U_f) and failure load (P_f), the sample loses its integrity through fiber breakage, matrix cracking, fiber-matrix pull-out, and delamination, bearing no more load. At the TP, the impact event ends, the load (P_t) decreases to zero, and the energy (U_t) has a constant value [36]. U_t is the total energy absorbed by the specimen and reflects the degree of induced and propagated damage [10]. The characteristic parameters were measured for three replicates and the average along with the standard deviation was reported in Table 1. The additional values in Table 1 are the normalized total absorbed energy (U_t/U), energy at maximum load (U_m/U), and elastic energy ($\Delta U/U$) retained in the indenter to rebound.

All the characteristic parameters including the normalized energy at the maximum load (U_m/U) increased with increasing impact energy, while the normalized absorbed (U_t/U) and elastic energies ($\Delta U/U$) did not vary. According to Ghaseminejhad and Parvizi-Majidi [38], the increase of contact loads and absorbed energies over higher impact energies are expected for 4.3 mm thick and 54% nominal fiber content CF-PEEK base material, once more potential energy of the indenter is converted into kinetic and transferred to the material through higher elastic-plastic deformation (U_m) and more internal damage (U_t). Despite the increases, typically for CF-PEEK, $\Delta U/U$ and U_m/U decrease with increasing impact energy, indicating that more energy is absorbed within the material – higher U_t/U – to initiate and propagate internal damages instead of elastic-plastic deformation [38]. For friction riveted joints however the increase of U_m/U and constant U_t/U may indicate a concealing of internal composite damage such as delamination and fiber breakage by elastic-plastic deformation of the joint materials as well as damage at the metal-composite interface, which were deeply investigated in Section 3.2.

At an impact energy of 5 J (Fig. 6-a) and 10 J (Fig. 6-b), the contact force signal presented oscillations, mainly in the descending part of the curves and P_i reached virtually similar values (approximately 7.5 kN), while at 20 J (Fig. 6-c) and 30 J (Fig. 6-d), featureless curves were observed along with higher P_i (9–11 kN). Such deviations in the behavior of the joints indicate differences in the damage mechanisms introduced by the impact load. As widely explored in the literature [1,2,10,18,37,39], discontinuities in impact force history address damage nucleation and propagation mainly by delamination and matrix

Table 1
Characteristic parameters of the dynamic response curves obtained from the drop weight impact test.

U [J]	P_i [kN]	U_i [J]	P_m [kN]	U_m [J]	P_f [kN]	U_f [J]	U_t [J]	U_t/U	U_m/U	$\Delta U/U$
5	5.4 ± 1.4	2.4 ± 0.6	7.3 ± 0.6	3.6 ± 0.2	5.8 ± 0.8	4.7 ± 0.05	4.3 ± 0.4	0.8 ± 0.008	0.7 ± 0.04	0.15 ± 0.04
10	7.5 ± 0.5	3.8 ± 0.4	14.2 ± 0.5	8.6 ± 0.2	9.5 ± 0.3	9.3 ± 0.06	7.1 ± 0.5	0.7 ± 0.05	0.8 ± 0.02	0.2 ± 0.05
20	8.8	4.7	14.4 ± 0.4	18.3 ± 0.1	14.2 ± 0.1	19.4 ± 0.0	14.6 ± 0.6	0.7 ± 0.03	0.9 ± 0.03	0.2 ± 0.03
30	11.4 ± 0.4	7.0 ± 0.5	18.7 ± 0.1	24.4 ± 4.0	16.4 ± 1.1	30.3 ± 0.01	24.0 ± 0.8	0.8 ± 0.02	0.9 ± 0.05	0.2 ± 0.02

cracking. In contrast, the featureless contact force signal may indicate no extensive failure of the composite by impact loading [40]. One can assume that the higher the impact energy, the larger the damaged area in the joint, especially in composites, which would result in more vibrations in the load curve. However, for hybrid friction riveted joints, similar to metal-composite laminates during an impact event [15], a featureless force-curve could indicate damage of the metal-composite interface, which in turn would lead to a different nature (elastic and/or plastic deformation) of damage, concealing the nucleation of flaws in the composite.

The relation between U and U_t determines the damage process imposed on the specimen from its contact with the indenter, which can be a rebound, penetration, or perforation [10]. On the one hand, when U_t is inferior to U the energy is partially released by elastic response, and therefore a rebound occurs. The relative elastic energy can be calculated as $\Delta U/U = (U - U_t)/U$. On the other hand, when the energies are equal the impact energy is completely released by damage to the material, inducing penetration of the indenter into the specimen. Perforation occurs when U_t no longer increases with U, meaning that the impact loading condition exceeds the load carrying capacity of the composite and the indenter passes through the thickness of the specimen. For all levels of impact energy investigated in this work, only the rebounding behavior was identified, as shown by Table 1.

The maximum load displays a nearly linear increase with low levels of impact energy ($U_i < 10$ J) before reaching a plateau between 10 J and 20 J at 14 kN, followed by an increase at the energy level of 30 J (Table 1). The plateau indicates a range of impact energies where the joint resists damage initiation mainly in the composite part. Such behavior is in turn dependent on the ductility of the matrix resin and the ability of the composite to resist initiation and propagation of delamination induced by mode II shear loading [41]. For composites, after the plateau the stiffness of the material usually decreases, leading to reduced load carrying capacity [37]. Contrary to the literature [37], the friction riveted joints show an increase in load carrying capacity towards 30 J, suggesting an additional damage mechanism releasing the energy, which complies with the findings in Fig. 6. Therefore, above 14 kN maximum force the damage mechanism to dissipate the impact energy changes from intralaminar and interlaminar damage in the composite to defects in the metal-composite interface. This observation does not necessarily mean a higher impact damage resistance of the joint upon higher impact energy, which in turn would not affect the joint's residual strength.

3.2. Impact damage

To assess the impact damage, a superficial area of damage (Fig. 7-a) and residual dent depth (Fig. 7-b) with increasing impact energy were investigated and the results are shown in Fig. 7-c. It is worth to mention that the damage modes and dimensions are strongly influenced by the temperature of the impact event [1,9] and the clamping system used to fix the sample, which effects were not investigated in the current paper.

By increasing the impact energy, shallow and larger superficial damage was observed. Moreover, two types of damage were identified for the friction riveted joints based on the dent depth criteria applied for aircraft composite structures [42,43]: barely visible impact damage (BVID) and visible impact damage (VID). According to the literature [6,44], when the damage has over 0.5 mm of residual dent depth, it is considered VID, while below this level it is BVID. At 5 J impact energy, a residual dent depth of 0.55 ± 0.06 mm was measured, and therefore considered the VID threshold for impacted friction riveted joints, below which BVID was defined. The 10 J impacted joints presented a residual dent depth of 0.8 ± 0.2 mm, which was virtually the same as for 5 J impacted joints, and consequently it was considered a transition energy level.

BVID and VID were inspected using SEM and CLSM along with the lateral view of friction riveted joints impacted with 5 J and 20 J, as shown in Fig. 8. The 5 J and 20 J were the first impact energy levels tested to induce BVID and VID, respectively, and therefore were selected for further microstructural analysis. At 5 J BVID was introduced and few cracks were observed in the impacted surface of the joint (arrow in Fig. 8-a). By contrast, in VID at 20 J the impacted surface exhibited a clear hemispherical indentation along with local crushing of the composite under the indenter and radial cracks (Fig. 8-b). The increasing of impact energy also led to detachment of the composite parts as shown by the comparison between Fig. 8-c and -d. This observation suggests that as the incident impact energy increases, a higher portion of such energy was absorbed within the joint through plastic deformation of the upper composite plate, which complies with the increase of U_m as well as the U_m/U ratio, as discussed in Section 3.1. Such deformation may induce peeling stress at the overlapped area promoting partial separation of the composite parts. It can be assumed that peeling stresses induced by impact accelerate the first failure mechanism of friction riveted joints under shear stress – i.e. rivet debonding from the lower composite part [26] – and hence decrease the load carrying capacity of

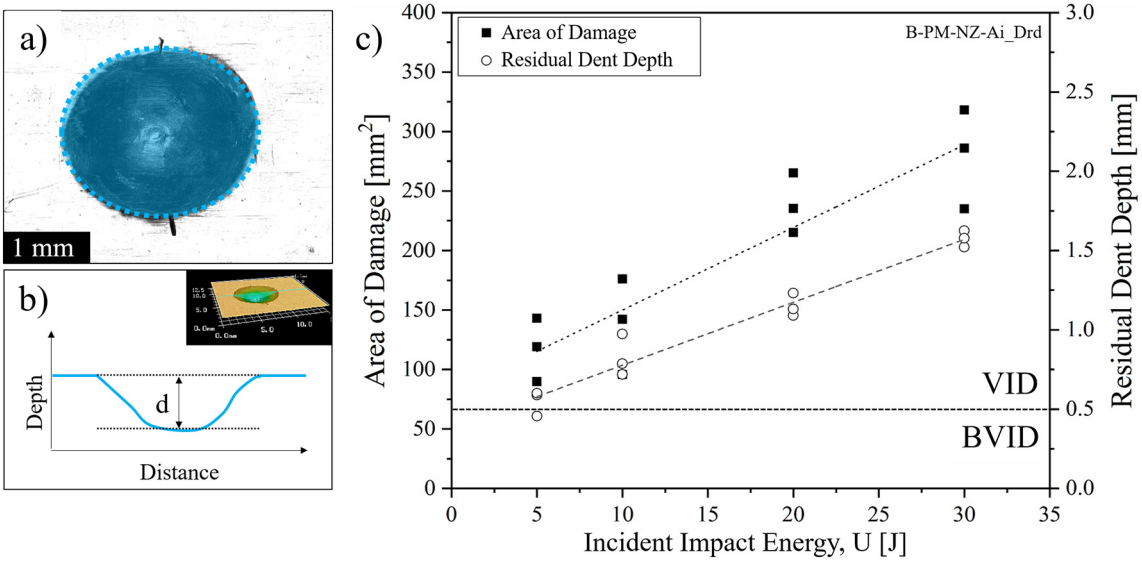

Fig. 7. Example of a) area of damage (A_i) and b) residual dent depth (d) measurements of friction riveted joints. c) Impact damage dimensions as a function of incident impact energy (5 J, 10 J, 20 J, and 30 J).

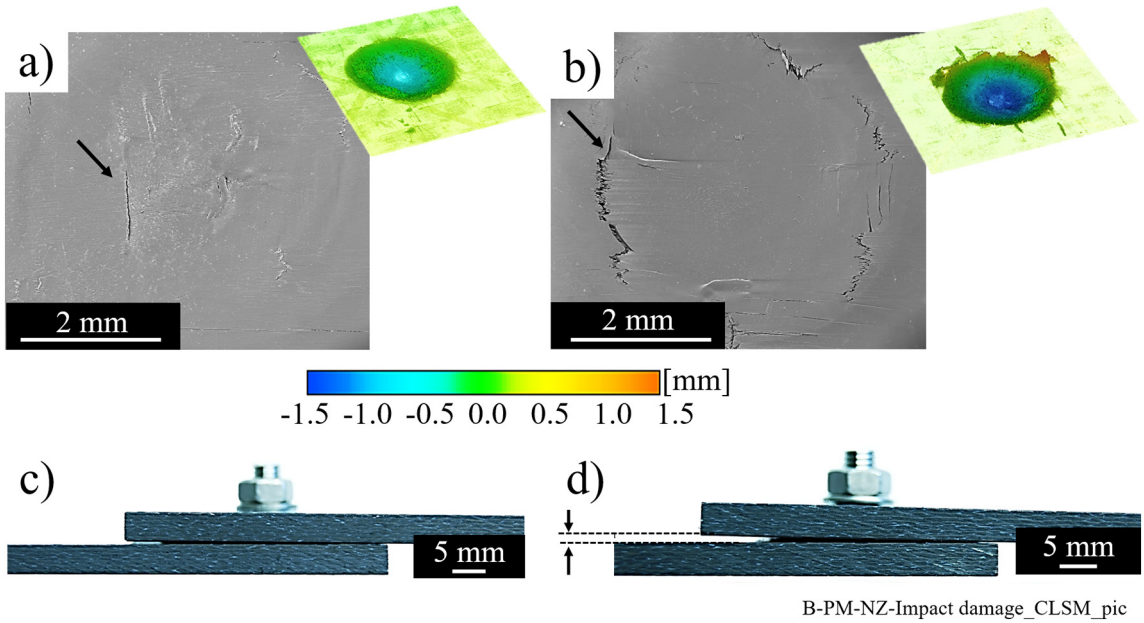

Fig. 8. SEM images along with 3D reconstructed images by CLSM of the impacted area with a) 5 J, and b) 20 J; side view of friction riveted joints impacted with c) 5 J, and d) 20 J, showing separation of the overlapped composite parts.

the joints. The negative contribution of the out-of-plane stresses over an impact event on the detachment of interfaces and failure of joints through CFRP delamination was already described by Harris and Adams [45] and Machado et al. [46] for adhesively bonded joints. Despite the larger imprint in the impacted composite surface with higher impact energy, no global distortion of the impacted composite plate was observed, which can be considered a result of localized damage favored by the woven fabric [1,39].

Considering the energy absorbed to create a unit of elastic/plastic deformation area – i.e. U_m/A_i – a friction riveted joint required from 96 kJ·m^{-2} to 273 kJ·m^{-2}, in a range of 5 to 30 J of incident impact energy, while a 4.3 mm thick and 54% nominal fiber content CF-PEEK requires between 39 kJ·m^{-2} to 62 kJ·m^{-2} in a similar incident impact energy range [38]. The result suggested that the presence of the metallic

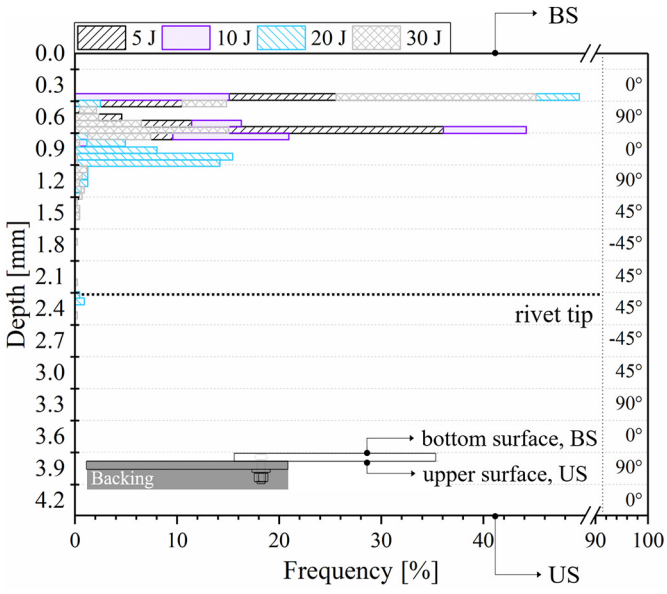

Fig. 9. Frequency of damage through the composite thickness as a function of incident impact energy. The insert schematic illustrates the positioning of the C-scan measurement, where BS stands for bottom surface and US for upper surface.

rivet in the impacted composite plate increases locally the stiffness of the composite, leading to an improvement up to four times of the required energy to further deform the composite.

The impacted composite joints also absorbs energy (see U_t in Table 1) internally to the composite leading to delamination, matrix cracks, and fiber breakage, which decrease the composite mechanical properties significantly [47]. Internal damage in the impacted friction riveted joints was assessed using the US C-Scan method. Fig. 9 shows the normalized frequency of detected defects through the thickness of the lower composite part over different impact energies. The composite thickness consists of 14 plies (thickness per ply = 0.31 mm [48]), the orientation of which is shown in the right hand side of the graph. The position of the rivet tip in the lower composite is also depicted in Fig. 9 by a horizontal dashed line. For all impact energy levels, the damage was accumulated mainly in the 0° and 90° plies located near to the impacted surface (bottom surface, BS). However, by increasing the impact energy from to 10 J and 30 J, the intensity of superficial damage increased (see first bar in Fig. 9). This can be explained by the radial propagation of cracks, as shown in Fig. 8-b. Additionally, at such levels, the damage was extended towards the surroundings of the rivet tip and detected in the ±45° plies at approximately 2.1 mm depth within the composite.

The qualitative result of the damage location in the composite was compared to the damage mechanisms taking place under low (5 J) and high (20 J) impact energy from the cross-section fractography, as presented in Fig. 10. At low impact energy, where a BVID was induced, cracks orientated at approximately 45° were detected in the first 0° ply which further propagated into the matrix (arrows in Fig. 10-b). One may assume that the detected cracks resulted from pure transverse shearing stress owing to the contact between the indenter and composite. Bieniaś et al. [15] reported a similar behavior with CFRP and aluminum hybrid laminates.

By examining the microstructure of 20 J impacted joints, it can be concluded that delamination is the prevailing damage mode in the VID. The failure of superficial plies was possibly governed by peeling stresses, leading to vertical cracks in the 0° plies, as shown in Fig. 10-c. In this case, the normal stresses in the layer plane may have overcome the transverse tensile strength of the layer. Fig. 10-d shows highly deflected crack in the 90° ply,

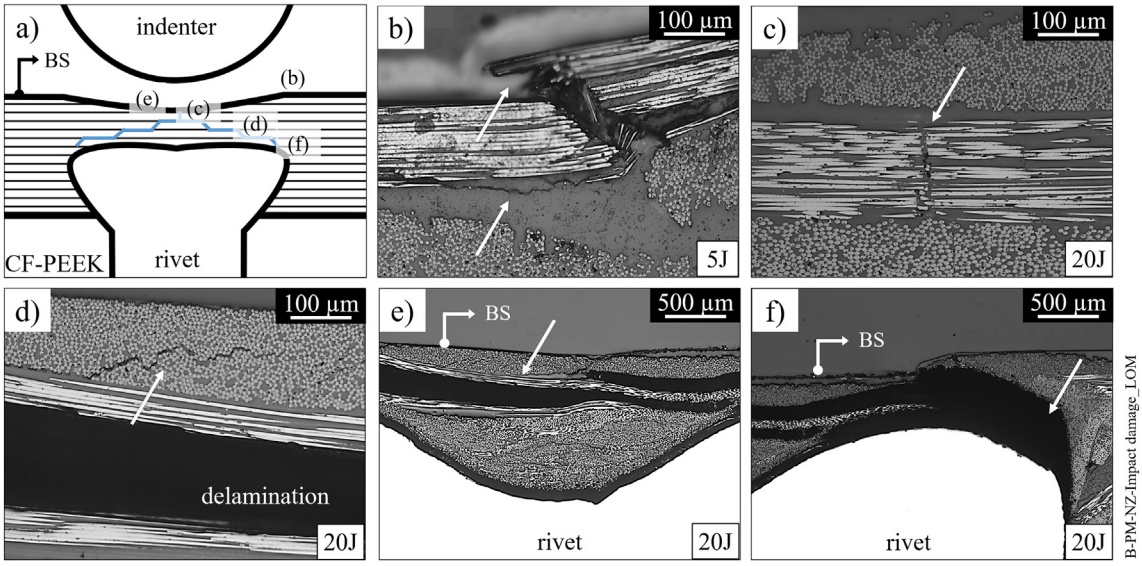

Fig. 10. a) Schematic illustration of the impacted friction riveted joint, depicting the main damage mechanisms under impact loading, which are detailed and highlighted by arrows in images b) to f): b) fiber failure under shear; c) fiber failure under tension; d) matrix cracking; e) delamination; f) interaction of delamination with the metal-composite interface.

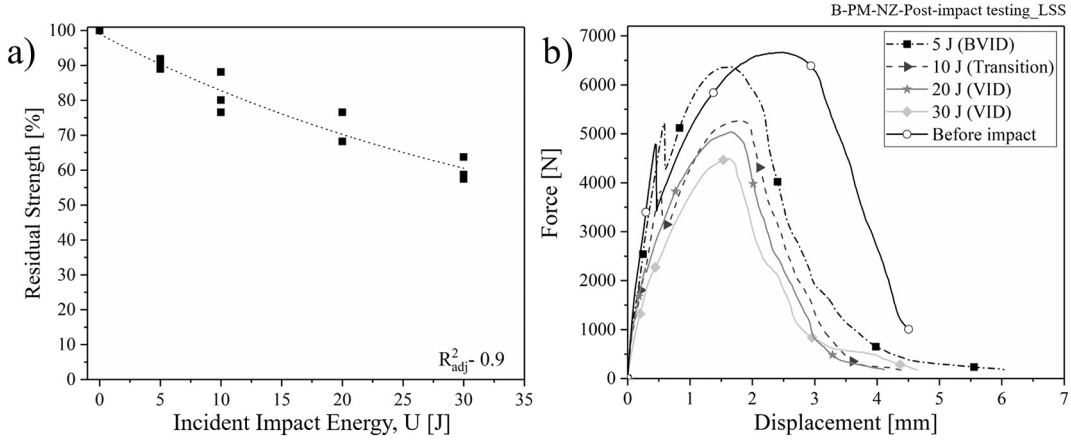

Fig. 11. a) Residual strength as a function of impact energy; b) typical load-displacement curves of friction riveted joints impacted with 5 J, 10 J, 20 J, and 30 J, compared with non-impacted specimens.

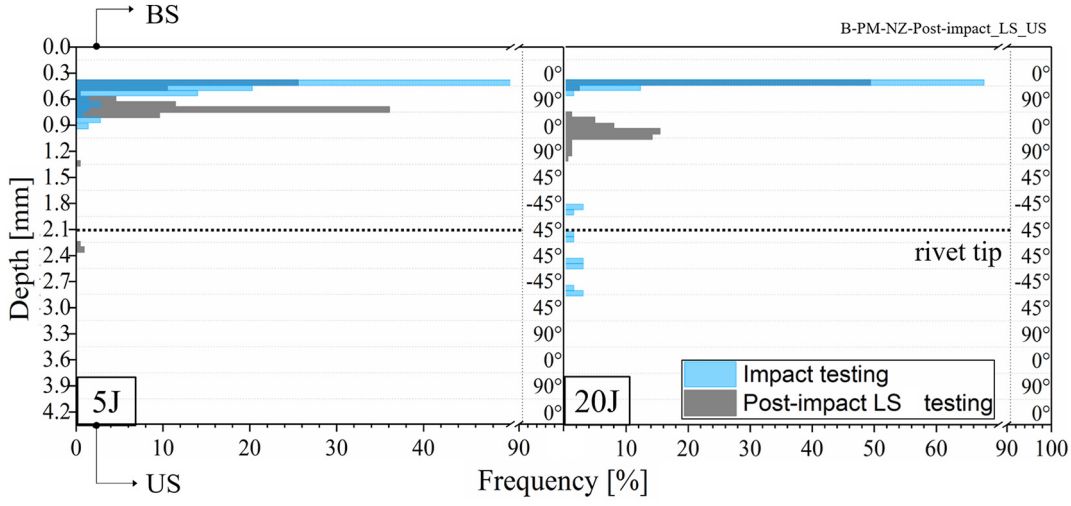

Fig. 12. Frequency of damage through the composite thickness of friction riveted joints impacted with 5 J and 20 J. BS stands for bottom surface while US stands for upper surface. The histogram shows the location of rivet tip penetration in the lower composite part.

which evolved into delamination mainly between 0° and 90° plies (Fig. 10-e) and propagated towards the metal-composite interface. The stacking sequence of 0° ply followed by 90° ply is more susceptible to delamination propagation, owing to the significant differences in their bending stiffness [15,49]. Fig. 10-f depicts the interaction between the delamination and the metal-composite interface, leading to complete fracture of the composite underneath the rivet, and consequently loss of joint integrity.

3.3. Post-impact quasi-static mechanical performance

Fig. 11-a shows residual strength under shear loading as a function of impact energy. Although compression is the critical load for composites [50], in-plane shear load is one of the most common scenarios that stiffened composite panels of aircraft fuselage are submitted to during flight [47]. Therefore, shear-after-impact (SAI) testing was carried out to investigate the effects of accidental damage on the joint strength.

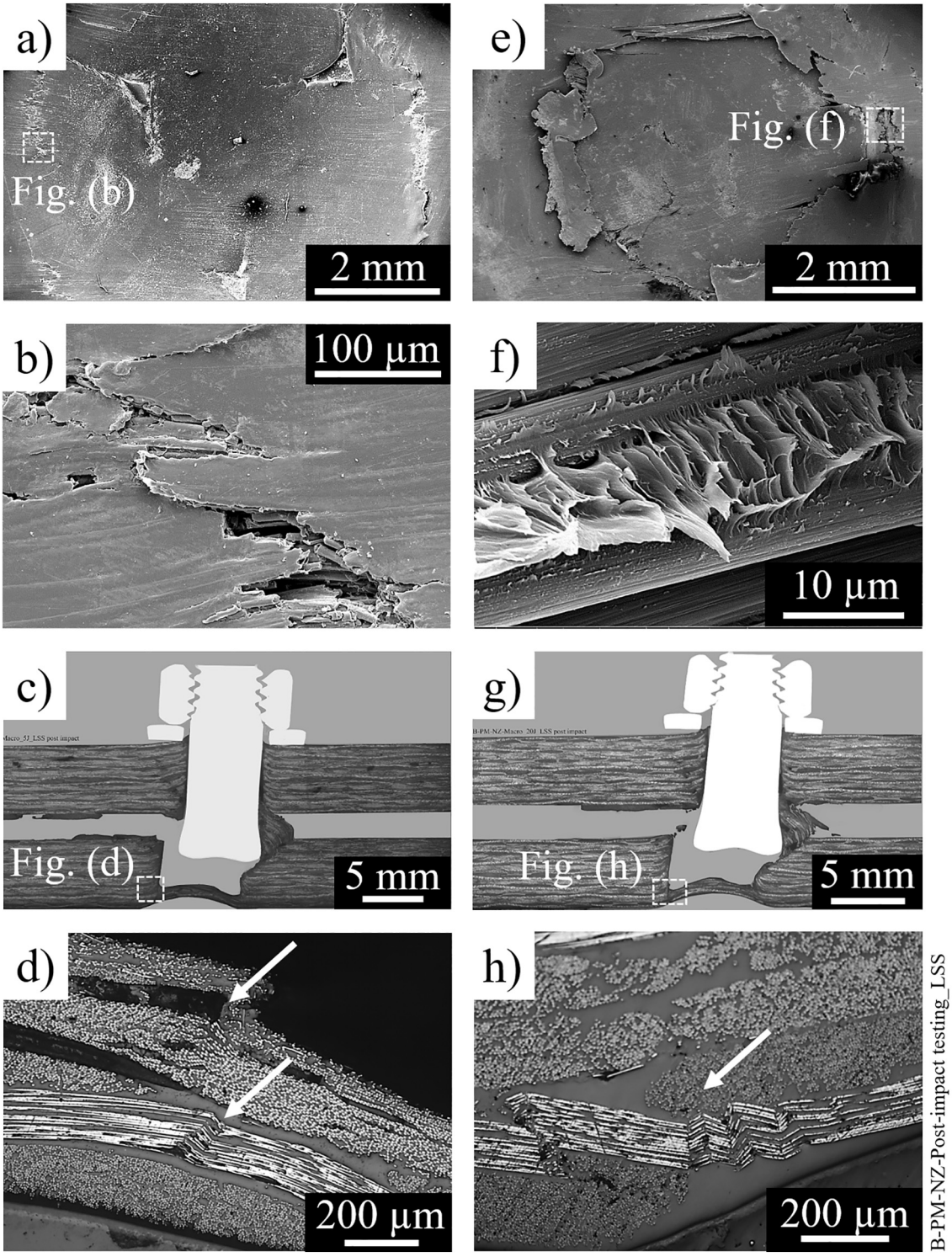

Fig. 13. Failure analysis of 5 J (a–d) and 20 J (e–h) impacted friction riveted joints after LS testing. a) SEM overview of the impacted area for 5 J; b) superficial cracking; c) typical cross-section of fractured joints impacted with 5 J; d) details of delamination and buckling of a 0° fiber bundle. e) SEM overview of the impacted area for 20 J; f) exposed tore fibrils at the impacted surface; g) typical cross-section of fractured joints impacted with 20 J; h) multiple kink-band in a 0° fiber bundle.

The residual strength was calculated from the ratio between the strength of damaged and non-impacted friction riveted joints. In the 5 J impacted joints, BVID was responsible for 9% decrease in the joint quasi-static strength, while for the VID resulting 30 J impact the decrease was down to 40%. The BVID result is way below the 19% decrease in quasi-static strength of 2 mm thickness CF-PEEK impacted with 3.9 J, as reported in [18], showing that the composite's impact tolerance may not be compromised by the joining process. In addition, a decrease in displacement at break and a change of the mechanical behavior towards final failure of the joints were observed in the typical force-displacement curves in Fig. 11-b. For the 5 J and 10 J impacted joints, the force-displacement curves display the characteristic two-peak behavior, typically described for the non-impacted friction riveted joints [26]. In such cases, the contribution of cohesive-adhesive failure of the squeezed polymeric material still provided an additional failure mechanism to arrest the energy prior to the crack propagation through the composite thickness triggered by shear stresses, meaning that this area remained intact. On the other hand, for the 20 J and 30 J impacted joints, the resulted peel stress (see Fig. 8-d) already damaged the squeezed material under tension and this no longer contributed to the joint's mechanical strength. Therefore, the load carrying capacity of such joints decreased drastically, leading to single-peak curves, as presented in Fig. 11-b.

The propagation of BVID and VID during a lap shear test was assessed by comparing the normalized frequency of detected damage through the thickness of the lower composite part, before and after the lap shear test, of 5 J and 20 J impacted joints, as presented in Fig. 12. The propagation of internal cracks introduced by 5 J impact energy essentially extended throughout the interface between the 0° and 90° plies (delamination), as well as on the composite surface and towards the surroundings of the rivet tip, where defects in the interface of ±45° plies were also detected. In the case of 20 J, the impact damage spread across all the composite plies, especially under intralaminar failure, as observed mainly by the damage accumulation internally to ±45° plies. It is important to emphasize that after lap shear (LS) testing, for both levels of impact energy, the impact damage interacted with the plastic deformation of the composite caused by bearing, which makes the assessment of impact damage propagation challenging. Similar to the friction riveted joints, Vander Klok et al. [51] reported difficulty in describing the evolution of damage mechanisms on an impacted metal-composite bolted joint.

Fig. 13 shows the dent areas along with the joint cross-section and fracture surface after LS testing for 5 J (Fig. 13-a to -d) and 20 J (Fig. 13-e to -h) impacted joints, respectively. An enlargement of the impacted area (Fig. 13-a) with pronounced shear-induced cracks near the surface of the composite (Fig. 13-b) was observed in the 5 J impacted joints, which complies with Fig. 12. A fully delaminated composite volume close to the composite hole is shown in Fig. 13-d. Such defects generated an empty volume in the composite that, when further compressed by the rivet, may better accommodate out-of-plane displacement of fiber bundles, especially 0° plies. This would explain the presence of a buckled 0° fiber bundle instead of a kink band formation (Fig. 13-d).

As well as enlargement of the impacted area (Fig. 13-e), the impacted surface of 20 J revealed exposed tore fibrils (Fig. 13-f), indicating the influence of secondary bending during LS testing on the impact damage propagation. The fiber and matrix breakage introduced by the impact (see Fig. 10) decreased the compression bearing capacity of the composite during LS testing which in turn promoted extensive out-of-plane displacement of the broken fibers in a 0° ply, resulting in multiple sites with a kink band, as shown in Fig. 13-h.

3.4. Post-impact fatigue behavior

Fig. 14-a shows the S-N curves of non-impacted and post-impacted friction riveted joints. The impact energies 5 J and 20 J were selected once they induced BVID and VID respectively. Post-impact fatigue testing defines the sensitivity of the structure to impact damage growth [50]. With increasing impact energy, a significant decrease in fatigue resistance was observed which complies with the lower residual quasi-static strength of 20 J impacted joints in comparison to 5 J impacted joints. As previously explained, in contrary to 5 J impacted joints, 20 J impacted joints underwent higher peeling stresses, leading to the premature adhesive failure of the squeezed material, which no longer contributed to joint strength. Moreover, the slope of the S-N curve for the higher impact energy was less steep than for the lower impact energy, indicating less dependency of the fatigue performance with the stress amplitude, once the joints were already severely damaged by the impact event.

To understand the post-impact fatigue behavior of friction riveted joints, the stiffness degradation over the fatigue life was monitored for 5 J and 20 J impacted joints and compared with non-impacted specimens, as shown in Fig. 14-b. The load level of 66% of the joint ULSF was selected based on an aircraft criterion, according to which, the fatigue life at 10^5 cycles is addressed to evaluate the performance and certify new joining technologies [52]. As reported by Borba et al. [26], in the case of non-impacted friction riveted joints, this fatigue life was reached with a stress amplitude of 56 MPa, which corresponded to load level of 66% of the ULSF.

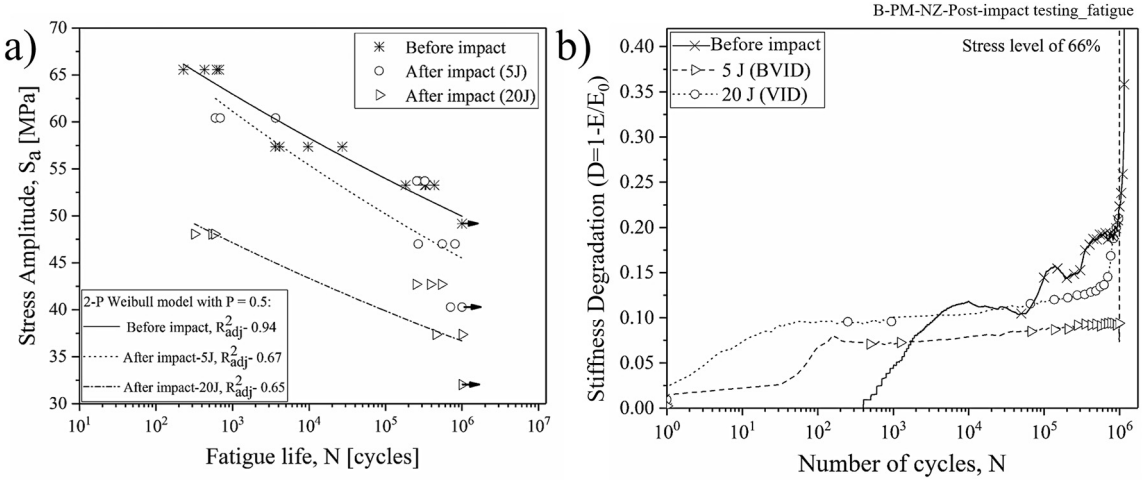

Fig. 14. a) S-N curves and b) stiffness degradation of friction riveted joints impacted with 5 J and 20 J. The stiffness degradation was evaluated for specimens loaded with 66% of their ULSF, to values as follows: $ULSF_{0J}$ - 6.6 ± 0.4 kN, $ULSF_{5J}$ - 6.0 ± 0.3 kN, $ULSF_{20J}$ - 4.8 ± 0.3 kN.

The joint stiffness degraded faster for 20 J impact energy in comparison to 5 J, which can be explained by the type of damage, its extent, and the effect of peel stresses induced by the impact testing. As previously discussed, the 20 J impacted joints presented shear-driven delamination (Fig. 10-d), which extended to the metal-composite interface, along with the failure of the squeezed material driven by peel stresses. According to Shahkhosravi et al. [53], delamination is a damage that propagates unstably and rapidly under fatigue testing. Therefore, one can assume that under low cycle fatigue the metal-composite interface failed entirely for the 20 J impacted joints, compromising the load transfer between the materials and hence inhibiting additional mechanisms to dissipate energy. The multiple modes of impact damage observed throughout the composite thickness in Fig. 10 for 20 J may also work as stress concentration sites that trigger faster damage propagation during fatigue testing. On the other hand, for 5 J impacted joints, in which no evidence of delamination and peeling defects were observed, it is expected that the squeezed material (Fig. 2-e) contributed to the resistance to low cycle fatigue. Consequently, the stiffness degradation rate is considerably inferior for 5 J impacted joints than for 20 J impacted joints up to 10^2 fatigue cycles.

In addition, at high cycle fatigue, where a plateau-like curve was established for both impact energy scenarios, unvarying stiffness degradation might indicate the contribution of the rivet to withstand the fatigue cycles. As the squeezed material and composite were progressively and prematurely degraded at low fatigue cycles, the undamaged rivet would partially arrest the crack that started propagating through the composite and metal-composite interface. Therefore, one can assume that the rivet plays a more important role in dissipating energy during cyclic testing in damaged joints compared to non-impacted joints, where the triggering of other failure mechanisms in the composite may occur.

By inspection of the fracture shown in Fig. 15, it can be drawn that the final failure in BVID joints under cyclic loading was not driven by the impact damage, despite it causing a reduction in their fatigue life (see Fig. 14). As highlighted by an arrow in Fig. 15-a, the composite underwent high plastic deformation, which enlarged the edges of the hole and assisted rivet removal from the composite part. This failure behavior is typical for non-impacted friction riveted joints under quasi-static and cyclic loading, as described in [26]. Additionally, hackles in the squeezed material confirm the plastic deformation of the squeezed material triggered by shear during fatigue testing (Fig. 15-c) [54]. VID joints are more prone to catastrophic failures, as evidenced by the low plastic deformation bore by the edges of the composite hole (Fig. 15-d) and intense cracking in the hole's surface (Fig. 15-e), mainly around

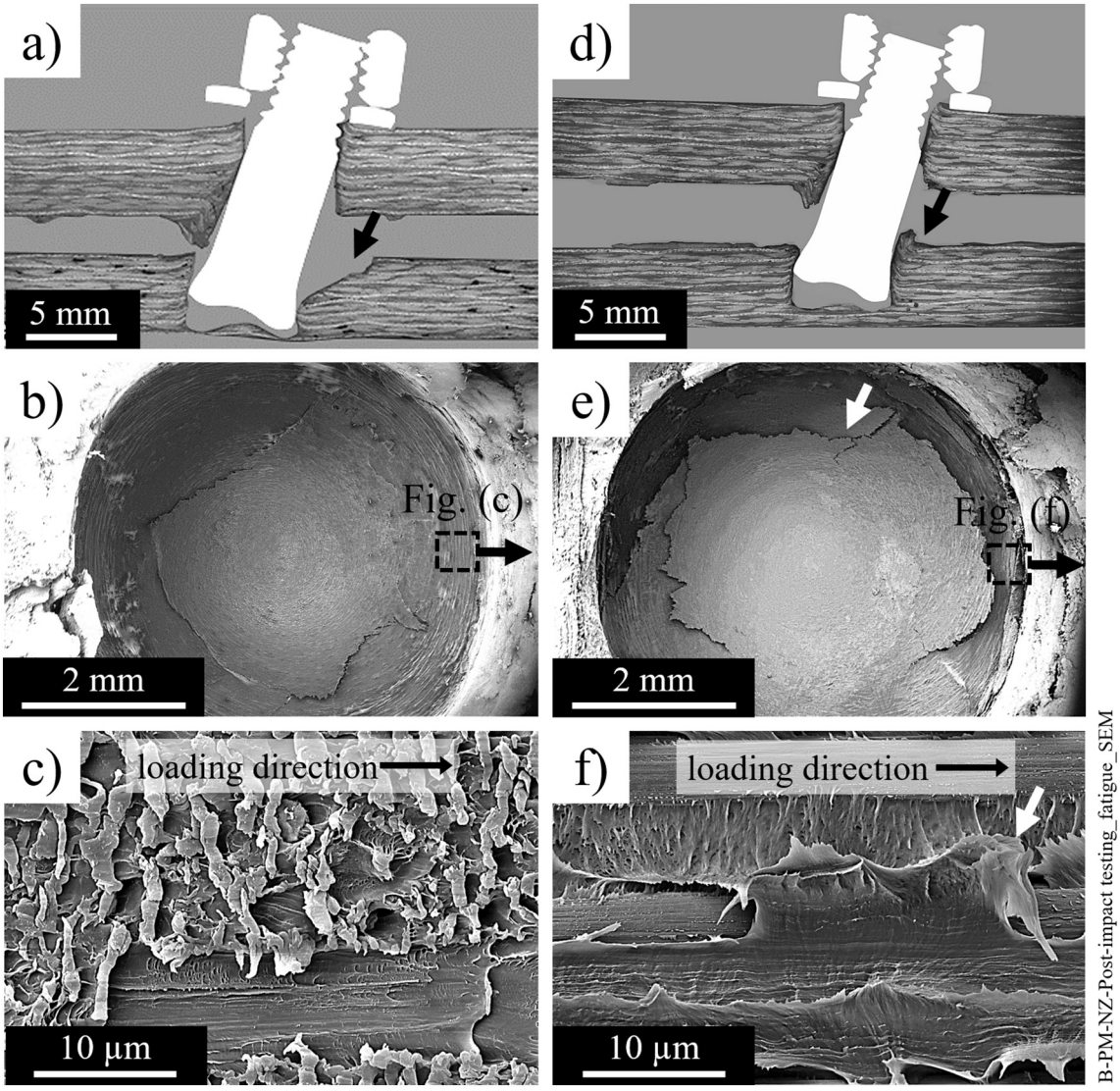

Fig. 15. a) Typical cross-section of failed friction riveted joint impacted with 5 J, along with b) overview of the composite hole and c) microstructure of the squeezed material, showing shear induced hackles. d) Typical cross-section of failed friction riveted joint impacted with 20 J along with e) overview of the composite hole and f) microstructure of the squeezed material showing tearing of fibrils.

the rivet tip, where the stress concentrations are believed to be higher under shear loading [55]. Fig. 15-f highlights the tearing of elongated fibrils in the squeezed material, confirming the influence of impact-induced peel stresses, which led to premature failure of the squeezed material prior to the cyclic loading.

The non-impacted and impacted specimens that survived 10^6 cycles (at least three replicates) were further tested under quasi-static loading to assess their residual strength, as shown in Fig. 16. According to the recommendations proposed for the damage tolerance analysis of composite aircraft structures, by EASA [42], it is necessary to ensure that such a structure is not exposed for an excessive period (fatigue cycles higher than 10^6 cycles), when it has a residual strength that is less than its design limit for loads. The residual strength of non-impacted and lower- and higher-energy impacted joints decreased by 9%, 2%, and 4% respectively. Although the fracture analysis showed a possible extension of the impact damage upon the fatigue cycles, their narrow variations in strength and standard deviation suggest that the effect of the cyclic loading on the initiation of additional damage by fatigue were not as critical to the joint mechanical integrity as the impact damage, either by BVID or by VID.

4. Conclusions

The current investigation assessed the sensitivity of Ti6Al4V/CF-PEEK friction riveted joints to different impact damage modes and to their propagation under quasi-static and cyclic loading. Overall, the presence of the metallic rivet in the impacted composite plate may increase locally the stiffness of the composite, leading to an improvement up to four times of the required energy to further damage the composite by elastic/plastic deformation. The higher the impact energy, the larger was the impact damage in the composite, which was characterized in two categories – barely-visible and visible impact damage – according to their residual dent depth. The 5 J impact energy introduced barely-visible impact damage with residual dent depth up to 0.5 mm and no indication of stress-driven delamination. Consequently, quasi-static and fatigue mechanical behavior were not significantly influenced. For impact energies above 5 J, visual impact damage was identified which combined delamination and premature failure of the metal-composite interface and squeezed material. Accordingly, the joint failure mode changed along with a decrease of up to 40% of the quasi-static joint strength, and low fatigue resistance. Under cyclic loading, the propagation of the impact damage showed to be less dependent on the stress amplitude, once the joints were already severely damaged by the impact event. Friction riveted joints showed to be less sensible to the fatigue damage than to the impact damage, as confirmed by the high residual strength after 10^6 fatigue cycles (98% and 96% for 5 J and 20 J, respectively). The empirical approach adopted in this work, including fundamental understanding of impact damage mechanisms, visual defect detectability, and assessment of residual strengths under different loading scenarios, has the potential to be further explored to aircraft composite structures and used to validate numerical analyzes for impact damage tolerance.

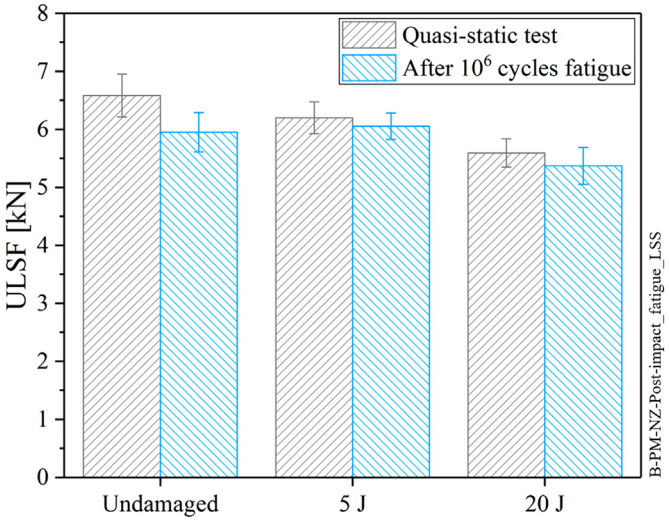

Fig. 16. Residual strength compared with the joint strength after one million fatigue cycles of non-impacted friction riveted joints and joints impacted with 5 J and 20 J.

CrediT authorship contribution statement

N.Z. Borba: Methodology, Formal analysis, Investigation, Writing - original draft. **J. Körbelin:** Resources, Visualization, Writing - review & editing. **B. Fiedler:** Resources, Writing - review & editing. **J.F. dos Santos:** Resources, Visualization. **S.T. Amancio-Filho:** Conceptualization, Supervision, Writing - review & editing.

Acknowledgments

This work was supported by the Helmholtz Association (Germany) and the National Council for Scientific and Technological Development - CNPq (Brazil) (grant number 200695/2015-0); S.T. Amancio-Filho would like to acknowledge “The Austrian aviation programme TAKE OFF” and “BMVIT-Austrian Ministry for Transport, Innovation and Technology” for his financial support.

Declaration of competing interest

The authors declared no conflicts of interest with respect to the research, authorship, and/or publication of this article. The raw/processed data required to reproduce these findings cannot be shared at this time due to technical or time limitations.

References

[1] Y. Wang, J. Zhang, G. Fang, J. Zhang, Z. Zhou, S. Wang, Influence of temperature on the impact behavior of woven-ply carbon fiber reinforced thermoplastic composites, Compos. Struct. 185 (2018) 435–445, https://doi.org/10.1016/j.compstruct.2017.11.056.
[2] J. Körbelin, M. Derra, B. Fiedler, Influence of temperature and impact energy on low velocity impact damage severity in CFRP, Compos. Part Appl. Sci. Manuf. 115 (2018) 76–87, https://doi.org/10.1016/j.compositesa.2018.09.010.
[3] T.K. Tsotsis, 8 - considerations of failure mechanisms in polymer matrix composites in the design of aerospace structures, Fail. Mech. Polym. Matrix Compos, Woodhead Publishing 2012, pp. 227–278 . http://www.sciencedirect.com/science/article/pii/B9781845697501500082 , (accessed March 16, 2017).
[4] G.A.O. Davies, X. Zhang, Impact damage prediction in carbon composite structures, Int. J. Impact Eng. 16 (1995) 149–170, https://doi.org/10.1016/0734-743X(94)00039-Y.
[5] G. Davies, R. Olsson, Impact on composite structures, Aeronaut. J. 108 (2004) 541–563, https://doi.org/10.1017/S0001924000000385.
[6] E. Morteau, V. Faivre, Damage tolerant composite fuselage sizing, FAST Mag. AIRBUS S.A.S 2011, pp. 10–16.
[7] B. Vieille, V.M. Casado, C. Bouvet, Influence of matrix toughness and ductility on the compression-after-impact behavior of woven-ply thermoplastic- and thermosetting-composites: a comparative study, Compos. Struct. 110 (2014) 207–218, https://doi.org/10.1016/j.compstruct.2013.12.008.
[8] S.H. Wang, M.D. Wei, L.W. Tsay, Tensile properties of LBW welds in Ti–6Al–4V alloy at evaluated temperatures below 450 °C, Mater. Lett. 57 (2003) 1815–1823, https://doi.org/10.1016/S0167-577X(02)01074-1.
[9] D. Garcia-Gonzalez, M. Rodriguez-Millan, A. Rusinek, A. Arias, Low temperature effect on impact energy absorption capability of PEEK composites, Compos. Struct. 134 (2015) 440–449, https://doi.org/10.1016/j.compstruct.2015.08.090.
[10] S. Boria, A. Scattina, G. Belingardi, Impact behavior of a fully thermoplastic composite, Compos. Struct. 167 (2017) 63–75, https://doi.org/10.1016/j.compstruct.2017.01.083.
[11] Z. Aslan, R. Karakuzu, B. Okutan, The response of laminated composite plates under low-velocity impact loading, Compos. Struct. 59 (2003) 119–127, https://doi.org/10.1016/S0263-8223(02)00185-X.
[12] J.J.M. Machado, P.M.-R. Gamarra, E.A.S. Marques, L.F.M. da Silva, Improvement in impact strength of composite joints for the automotive industry, Compos. Part B Eng. 138 (2018) 243–255, https://doi.org/10.1016/j.compositesb.2017.11.038.
[13] S.-S. Pang, C. Yang, Y. Zhao, Impact response of single-lap composite joints, Compos. Eng. 5 (1995) 1011–1027, https://doi.org/10.1016/0961-9526(95)00003-6.

[14] E. Ghanbari, O. Sayman, Y. Pekbey, O. Ozdemir, Experimental analysis of single-lap composite joints with two different adhesives at various conditions, J. Compos. Mater. 50 (2016) 1709–1715, https://doi.org/10.1177/0021998315595532.

[15] J. Bieniaś, P. Jakubczak, B. Surowska, K. Dragan, Low-energy impact behaviour and damage characterization of carbon fibre reinforced polymer and aluminium hybrid laminates, Arch. Civ. Mech. Eng. 15 (2015) 925–932, https://doi.org/10.1016/j.acme.2014.09.007.

[16] J. Reiner, J.P. Torres, M. Veidt, M. Heitzmann, Experimental and numerical analysis of drop-weight low-velocity impact tests on hybrid titanium composite laminates, J. Compos. Mater. 50 (2016) 3605–3617, https://doi.org/10.1177/0021998315624002.

[17] P. Viegas Ochoa de Carvalho, R.M. Groves, R. Benedictus, Full-scale testing of an ultrasonic guided wave based structural health monitoring system for a thermoplastic composite aircraft primary structure, EWSHM 2018 9th Eur. Workshop Struct. Health, 2018. http://resolver.tudelft.nl/uuid:98088174-5098-445f-835d-98363e193ed6, Accessed date: 30 November 2018.

[18] N.-H. Tai, M.-C. Yip, C.-M. Tseng, Influences of thermal cycling and low-energy impact on the fatigue behavior of carbon/PEEK laminates, Compos. Part B Eng. 30 (1999) 849–865, https://doi.org/10.1016/S1359-8368(99)00048-7.

[19] N.Z. Borba, L. Blaga, J.F. dos Santos, S.T. Amancio-Filho, Direct-friction riveting of polymer composite laminates for aircraft applications, Mater. Lett. 215 (2018) 31–34, https://doi.org/10.1016/j.matlet.2017.12.033.

[20] N.Z. Borba, J.F. dos Santos, S.T. Amancio-Filho, The influence of clamping pressure on joint formation and mechanical performance of Ti6Al4V/CF-PEEK friction-riveted joints, Materials 12 (2019) 745, https://doi.org/10.3390/ma12050745.

[21] J. Altmeyer, U.F.H. Suhuddin, J.F. dos Santos, S.T. Amancio-Filho, Microstructure and mechanical performance of metal-composite hybrid joints produced by FricRiveting, Compos. Part B Eng. (2015) 130–140.

[22] J. Altmeyer, J.F. dos Santos, S.T. Amancio-Filho, Effect of the friction riveting process parameters on the joint formation and performance of Ti alloy/short-fibre reinforced polyether ether ketone joints, Mater. Des. 60 (2014) 164–176, https://doi.org/10.1016/j.matdes.2014.03.042.

[23] L. Blaga, J.F. dos Santos, R. Bancila, S.T. Amancio-Filho, Friction riveting (FricRiveting) as a new joining technique in GFRP lightweight bridge construction, Constr. Build. Mater. 80 (2015) 167–179, https://doi.org/10.1016/j.conbuildmat.2015.01.001.

[24] B. Proença, L. Blaga, L.B. Canto, J.F. Dos Santos, S.T. Amancio-Filho, Force Controlled Friction Riveting of Glass Fiber Reinforced Polyamide 6 and Aluminum Alloy 6056 Hybrid Joints, Orlando 2015.

[25] N.Z. Borba, C.R.M. Afonso, L. Blaga, J.F. dos Santos, L.B. Canto, S.T. Amancio-Filho, On the process-related rivet microstructural evolution, material flow and mechanical properties of Ti-6Al-4V/GFRP friction-riveted joints, Materials 10 (2017) 184, https://doi.org/10.3390/ma10020184.

[26] N.Z. Borba, B. Kötter, B. Fiedler, J.F. Dos Santos, S.T. Amancio-Filho, Mechanical integrity of friction-riveted joints for aircraft applications, Compos. Struct. 232 (2020), 111542. https://doi.org/10.1016/j.compstruct.2019.111542.

[27] G. Pina Cipriano, L.A. Blaga, J.F. dos Santos, P. Vilaça, S.T. Amancio-Filho, Fundamentals of force-controlled friction riveting: part I—joint formation and heat development, Materials 11 (2018) 2294, https://doi.org/10.3390/ma11112294.

[28] G. Pina Cipriano, L.A. Blaga, J.F. dos Santos, P. Vilaça, S.T. Amancio-Filho, Fundamentals of force-controlled friction riveting: part II—joint global mechanical performance and energy efficiency, Materials 11 (2018) 2489, https://doi.org/10.3390/ma11122489.

[29] U.A. Khashaba, H.E.M. Sallam, A.E. Al-Shorbagy, M.A. Seif, Effect of washer size and tightening torque on the performance of bolted joints in composite structures, Compos. Struct. 73 (2006) 310–317, https://doi.org/10.1016/j.compstruct.2005.02.004.

[30] C.F. Rodrigues, L.A. Blaga, J.F. dos Santos, L.B. Canto, E. Hage, S.T. Amancio-Filho, FricRiveting of aluminum 2024-T351 and polycarbonate: temperature evolution, microstructure and mechanical performance, J. Mater. Process. Technol. 214 (2014) 2029–2039, https://doi.org/10.1016/j.jmatprotec.2013.12.018.

[31] S.T. Amancio-Filho, Henry Granjon Prize Competition 2009 Winner Category A: "Joining and Fabrication Technology" Friction Riveting: Development and Analysis of a New Joining Technique for Polymer-Metal Multi-Material Structures, 55, Weld. World, 2011 13–24, https://doi.org/10.1007/BF03263511.

[32] ASTM International, ASTM D7136/D7136M-15, Standard Test Method for Measuring the Damage Resistance of a Fiber-Reinforced Polymer Matrix Composite to a Drop-Weight Impact Event, West Conshohocken, PA, 2015https://doi.org/10.1520/D7136_D7136M-15.

[33] ASTM D5961, Standard Test Method for Bearing Response of Polymer Matrix Composite Laminates, 2017.

[34] ASTM International, ASTM E739 - 10 Standard Practice for Statistical Analysis of Linear or Linearized Stress-Life, West Conshohocken, PA, https://www.astm.org/Standards/E739 2015, Accessed date: 3 September 2019.

[35] DIN - German Institute for Standardization, DIN 50100:2016-12, Standard Load Controlled Fatigue Testing - Execution and Evaluation of Cyclic Tests at Constant Load Amplitudes on Metallic Specimens and Components, 2016.

[36] M.N. Ghaseminejhad, A. Parvizi-Majidi, Impact behaviour and damage tolerance of woven carbon fibre-reinforced thermoplastic composites, Constr. Build. Mater. 4 (1990) 194–207, https://doi.org/10.1016/0950-0618(90)90040-8.

[37] S.-L. Gao, J.-K. Kim, Cooling rate influences in carbon fibre/PEEK composites. Part III: impact damage performance, Compos. Part Appl. Sci. Manuf. 32 (2001) 775–785, https://doi.org/10.1016/S1359-835X(00)00189-5.

[38] M.N. Ghasemi Nejhad, A. Parvizi-Majidi, Impact behaviour and damage tolerance of woven carbon fibre-reinforced thermoplastic composites, Composites 21 (1990) 155–168, https://doi.org/10.1016/0010-4361(90)90008-K.

[39] B. Vieille, V.M. Casado, C. Bouvet, About the impact behavior of woven-ply carbon fiber-reinforced thermoplastic- and thermosetting-composites: a comparative study, Compos. Struct. 101 (2013) 9–21, https://doi.org/10.1016/j.compstruct.2013.01.025.

[40] G. Minak, Z. Šoški, Characterization of Impact Behavior of Composite Car Components, 2011.

[41] R. Bogenfeld, J. Kreikemeier, T. Wille, Review and benchmark study on the analysis of low-velocity impact on composite laminates, Eng. Fail. Anal. 86 (2018) 72–99, https://doi.org/10.1016/j.engfailanal.2017.12.019.

[42] European Aviation Safety Agency - EASA, Certification Specifications for Large Aeroplanes (CS-25), (n.d.) 617.

[43] S. Mustapha, L. Ye, X. Dong, M.M. Alamdari, Evaluation of barely visible indentation damage (BVID) in CF/EP sandwich composites using guided wave signals, Mech. Syst. Signal Process. 76–77 (2016) 497–517, https://doi.org/10.1016/j.ymssp.2016.01.023.

[44] A. Singh, B. Davidson, D. Eisenberg, M. Czabaj, A. Zehnder, Barely visible impact damage evaluation of composite sandwich structures, 51st AIAAASMEASCEAHSASC Struct. Struct. Dyn. Mater. Conf., American Institute of Aeronautics and Astronautics, 2010https://doi.org/10.2514/6.2010-2770.

[45] J.A. Harris, R.D. Adams, An assessment of the impact performance of bonded joints for use in high energy absorbing structures, Proc. Inst. Mech. Eng. Part C J. Mech. Eng. Sci. 199 (1985) 121–131, https://doi.org/10.1243/PIME_PROC_1985_199_102_02.

[46] J. Machado, E. Marques, L. da Silva, Mechanical behaviour of adhesively bonded composite single lap joints under quasi-static and impact conditions with variation of temperature and overlap, J. Compos. Mater. 52 (2018) 3621–3635, https://doi.org/10.1177/0021998318766641.

[47] P.E. Irving, C. Soutis, Polymer Composites in the Aerospace Industry, Elsevier, 2014https://doi.org/10.1016/C2013-0-16303-9.

[48] Toho Tenax, Teijin, Tenax®-E TPCL PEEK-HTA40 product data sheet, n.d. http://www.tohotenax.com/pt/produtos/tenax%c2%ae-composites/tenax%c2%ae-thermoplastics/, Accessed date: 20 June 2017.

[49] Damage in laminates from low-velocity impacts, Dyn. Deform. Damage Fract. Compos. Mater. Struct 2016, pp. 35–69, https://doi.org/10.1016/B978-0-08-100080-9.00003-8.

[50] L.G. Melin, J. Schön, T. Nyman, Fatigue testing and buckling characteristics of impacted composite specimens, Int. J. Fatigue 24 (2002) 263–272, https://doi.org/10.1016/S0142-1123(01)00081-0.

[51] A. VanderKlok, A. Dutta, S.A. Tekalur, Metal to composite bolted joint behavior evaluated at impact rates of loading, Compos. Struct. 106 (2013) 446–452, https://doi.org/10.1016/j.compstruct.2013.06.004.

[52] H.S.B. Schmidt-Brandecker, Fatigue & Damage Tolerance, 2017.

[53] N.A. Shahkhosravi, J. Yousefi, M.A. Najafabadi, C. Burvill, G. Minak, Fatigue life reduction of GFRP composites due to delamination associated with the introduction of functional discontinuities, Compos. Part B Eng. (2019) https://doi.org/10.1016/j.compositesb.2019.01.005.

[54] A. Plumtree, L. Shi, Fatigue damage evolution in off-axis unidirectional CFRP, Int. J. Fatigue 24 (2002) 155–159, https://doi.org/10.1016/S0142-1123(01)00068-8.

[55] M.F. Borges, S.T. Amancio-Filho, J.F. dos Santos, T.R. Strohaecker, J.A.E. Mazzaferro, Development of computational models to predict the mechanical behavior of friction riveting joints, Comput. Mater. Sci. 54 (2012) 7–15, https://doi.org/10.1016/j.commatsci.2011.10.031.